



# Acoustic Waves in a High-Temperature Plasma II. Damping and Instability

B.B. Mikhalyaev<sup>1</sup> · S.B. Derteev<sup>1</sup> · N.K. Shividov<sup>1</sup> · M.E. Sapraliev<sup>1</sup> · D.B. Bembitov<sup>1</sup>

Received: 22 December 2022 / Accepted: 9 August 2023 / Published online: 4 September 2023  
© The Author(s), under exclusive licence to Springer Nature B.V. 2023

## Abstract

In this article we study the properties of acoustic waves in the rarefied high-temperature plasma of the solar corona, assuming that the heating and cooling of the plasma has a well-defined description. We consider a constant heating function supposing that the heating processes are generally established. For the radiative-loss function, a number of values are taken, which have been found using the CHIANTI code. On their basis, an analytical expression of the function in the form of a cubic interpolation has been worked out. We analyze the dispersion relation for linear acoustic waves. The heating and cooling function, introduced along with the classical expression of the thermal conductivity, allows us to obtain some specific results about their properties. In other words, a model of non-adiabatic acoustic waves with field-aligned thermal conduction, CHIANTI-based radiative cooling and constant heating function is constructed. Using the available observational data on compression waves, we can set the problem of finding the parameters of the coronal plasma. The model allows to specify the temperature range at which the thermal instability of waves is possible and to draw some conclusions about their damping. The coronal temperatures considered can be divided into intervals from 0.5 to 0.98 MK and from 4.57 to 8.38 MK, where the radiation function increases, and intervals from 0.98 to 4.57 MK and from 8.38 to 10 MK, where the radiation function decreases. With constant heating, at large wavelengths, acoustic waves can be unstable in the decreasing interval from 1.38 to 3.15 MK. In the increasing intervals, they may have a zero real part of the oscillation frequency and thus become non-propagating, also subject to a large wavelength. In some cases, the plasma density has a significant effect on the damping of acoustic oscillations due to heating and cooling. A change in density within the same order can lead to the fact that the heating and cooling effects prevail over the effect of thermal conductivity on long-wave perturbations.

**Keywords** Corona · Coronal seismology · Heating, coronal · Waves, acoustic · Instabilities

---

✉ B.B. Mikhalyaev  
[bbmikh@mail.ru](mailto:bbmikh@mail.ru)

S.B. Derteev  
[derteevsergei@gmail.com](mailto:derteevsergei@gmail.com)

<sup>1</sup> Department of Theoretical Physics, Kalmyk State University named after B.B. Gorodovikov, Elista, Russia

## 1. Introduction

One of the important topics of solar physics is the study of compression waves, which are observed everywhere in the lower corona by variations in the intensity of the plasma radiation (Srivastava et al. 2008; De Moortel 2009; Banerjee, Gupta, and Teriaca 2011; Krishna Prasad, Banerjee, and Gupta 2011; De Moortel and Nakariakov 2012; Banerjee and Krishna Prasad 2016; Wang 2016; Krishna Prasad and Van Doorselaere 2021). They are theoretically described as slow or acoustic waves. The acoustic waves can provide useful information about the parameters of the coronal plasma (Wang 2011; De Moortel and Nakariakov 2012) or indicate the sources of its heating (Taroyan and Erdélyi 2009). The mechanisms of wave energy dissipation and their efficiency are also of interest. The list of works on this topic is very extensive, so we often refer to review papers.

Except for the solar wind, the energy losses of the coronal plasma are due to thermal conductivity and radiation (Narain and Ulmschneider 1996). Kumar, Nakariakov, and Moon (2016), Krishna Prasad, Banerjee, and Van Doorselaere (2014) and Prasad, Srivastava, and Wang (2021) examined the heating and cooling effect, thermal conductivity and viscosity on compression waves in coronal loops. Sometimes thermal conductivity and viscosity are taken into account (Ofman and Wang 2002, De Moortel and Hood 2003), but more often thermal conductivity and heating and cooling are considered (Carbonell, Oliver, and Ballester 2004; Soler, Ballester, and Goossens 2011; Kolotkov, Nakariakov, and Zavershinskii 2019; Duckenfield, Kolotkov, and Nakariakov 2021). The aim of this article is to find out whether heating and cooling can have a noticeable effect on the damping of acoustic waves in comparison with thermal conductivity and in what situations this is possible. It has been noted that the radiative loss can have a noticeable effect on the oscillations of coronal loops (Priest et al. 1998; Aschwanden and Terradas 2008). In the solar corona, radiation affects the slow waves more strongly than the fast waves (Mikhalyaev, Veselovskii, and Khongorova 2013). Absorption of wave energy due to thermal conductivity leads not only to damping of the acoustic wave, but also to its dispersion. In practice, this should lead to the appearance of quasi-periodic oscillations generated as a result of the spreading of the initial localized perturbation. A misbalance between heating and radiative losses has a similar effect on the wave (Zavershinskii et al. 2019; Belov, Molevich, and Zavershinskii 2021).

We use the values of the radiative-loss function calculated with the help of the well-known CHIANTI code (Dere et al. 2009; Dudík et al. 2011; Del Zanna et al. 2021). Using the cubic spline interpolation method, an approximate analytical expression of this function is formulated, which is then used in the analysis of a linear acoustic wave. We consider the heating function to be constant. This is acceptable when the heating processes are of a stable nature or they give a constant supply of energy on average, so that their spatial and temporal scales are large compared with the wave scales. The approximation of constant heating is often used in the study of wave processes, since in specific situations it is not possible to define the sources and nature of the energy supply (Parker 1953; Weymann 1960; Priest 2014). The number of possible sources is very large (Narain and Ulmschneider 1996; Erdélyi and Ballai 2007; Klimchuk 2015). There is evidence to confirm a steady heating concept (Warren, Winebarger, and Brooks 2010; Tripathi, Klimchuk, and Mason 2011).

Thus, in our case, the function of heating and energy losses is strictly defined. For thermal conductivity, the classical expression is used, which is valid for fully ionized plasma (Spitzer 1962). We can say that a specific model of the non-adiabatic acoustic waves has been adopted, which makes it possible to find definite physical conditions for the wave and compare results with observational data. Due to the physical model specificity we can estimate the parameters of the coronal plasma. The CHIANTI radiative-loss function was used

to study the damping of slow waves in hot coronal loops (Kolotkov, Nakariakov and Zavershinskii 2019) and in prominences (Ibañez and Ballester 2022). Zavershinskii et al. (2019) considered the heating and cooling misbalance as a source of quasi-periodic coronal oscillations. The proposed new analytical CHIANTI function representation provides a clear and systematic approach to study the heating and cooling effect on the behavior of acoustic waves in the corona at all permissible values of basic physical parameters, density and temperature. Thus, it is possible to clarify some results concerning the conditions for the occurrence of acoustic wave instability and damping, to find exactly the conditions when the heating and cooling effect plays a significant role in the damping along with the thermal conductivity. In some papers, the object of the study is the heating and cooling function itself (Kolotkov, Duckenfield, and Nakariakov 2020; Kolotkov, Zavershinskii, and Nakariakov 2021).

The study carried out in our work appears to be in agreement with the general work of Field (1965), where, along with the acoustic waves, condensation modes are considered. Field introduced the minimum number of formal parameters into the dispersion relation, namely, two, and found the region of instability on the plane of these parameters. This choice is due to the general representation of the heating and cooling function. Our model allows us to choose the density  $\rho_0$  and the temperature  $T_0$  of the equilibrium plasma as the basic parameters and then follow the behavior of the wave depending on these parameters.

We are planning to prepare a series of papers on the topic of the damping and dispersion of acoustic waves. Since we want to propose a certain mathematical model, we present its theoretical foundations in detail and consider its application to numerous examples of compression wave observations in the solar corona. Our first paper is devoted to a detailed description of the CHIANTI radiative-loss function interpolation (Derteev et al. 2023); we will refer to it as Paper I. This work is a continuation and is referred to as Paper II. We now focus on the behavior of acoustic waves at different values of plasma density and temperature. We show at what temperatures wave instability is possible and the degree of its damping at other temperatures. We discuss a form of the heating and cooling function in Section 2. We give brief explanations of the interpolation in Section 3. We present basic equations in Section 4. We focus on the phenomena of instability in Section 5 and damping in Section 6. In this article we discuss the application of the model to standing waves in hot coronal loops.

## 2. Heating and Cooling Functions

Here we discuss the description of the coronal plasma heating and cooling processes. In many papers a suitable expression for the heating and cooling function is discussed, but so far it has not been defined even for specific cases. We try to clarify the uncertainty that exists in this matter.

The energy emitted by a rarefied coronal plasma per unit mass and time may be expressed as (Weymann 1960; Hildner 1974, Somov and Syrovatskij 1980)

$$Q_{\text{rad}} = \rho \Lambda(T), \quad (1)$$

where  $\Lambda(T)$  is the optically thin radiative-loss function. A large number of papers are devoted to its study, because of both the importance of the role of radiation in many physical processes in the solar atmosphere and, to a large extent, the ambiguity of its definition. The latter, in turn, is explained by the inhomogeneity of the atmosphere and the current uncertainty in the distribution of ions. Currently, the radiative-loss function obtained using the

CHIANTI code has become very popular (Dere et al. 1997; Landi et al. 1999; Dere et al. 2009; Dudík et al. 2011).

Although the behavior of the radiative-loss function is well known in general, in the study of wave phenomena, not enough attention is paid to its specific properties. In the case where the plasma density and temperature vary within small intervals, a local power-law approximations of the form

$$\Lambda(T) = \chi T^\alpha, \quad \chi, \alpha \text{ are constants,} \tag{2}$$

can be used (Rosner, Tucker, and Vaiana 1978; De Moortel and Hood 2004; Carbonell, Oliver, and Ballester 2004; Krishna Prasad, Banerjee, and Van Doorselaere 2014; Wang et al. 2021). In the work of Klimchuk, Patsourakos, and Cargill (2008) a global approximation is given, which is constructed in this way for seven local ranges:

$$\rho^2 \Lambda(T)/n^2 = \begin{cases} 1.09 \cdot 10^{31} T^2, & T \leq 10^{4.97}, \\ 8.87 \cdot 10^{17} T, & 10^{4.97} \leq T \leq 10^{5.67}, \\ 1.90 \cdot 10^{22}, & 10^{5.67} \leq T \leq 10^{6.18}, \\ 3.53 \cdot 10^{13} T^{3/2}, & 10^{6.18} \leq T \leq 10^{6.55}, \\ 3.46 \cdot 10^{25} T^{1/3}, & 10^{6.55} \leq T \leq 10^{6.90}, \\ 5.49 \cdot 10^{16} T, & 10^{6.90} \leq T \leq 10^{7.63}, \\ 1.96 \cdot 10^{27} T^{1/2}, & 10^{7.63} \leq T. \end{cases} \tag{3}$$

Although such expressions are quite suitable for describing infinitesimal perturbations, a more precise expression is required when studying small finite perturbations. Moreover, they do not reflect the detailed behavior of the radiative-loss function. We use the radiative-loss data obtained using the CHIANTI 10 code (Del Zanna et al. 2021) and calculate a more accurate expression through cubic spline interpolation, which gives the continuity of the first and second function derivatives over the entire temperature range under consideration.

Unlike, for example, loss due to thermal conductivity, which disappears in a homogeneous equilibrium medium with no temperature gradient, radiative loss occurs. Therefore, when modeling wave processes, along with radiative loss, sources of plasma heating are usually considered, introducing the heating and cooling functions

$$Q_{hc} = Q_{rad} - H, \tag{4}$$

where  $H$  is the heating function, which has the meaning of energy inflow due to various reasons. It should be expected that in the absence of a wave, there is a balance between the radiation energy losses and energy inflow from possible heating sources. The large number of these sources and the uncertainty of their description (De Moortel and Browning 2015; Klimchuk 2015) make this balance “one of the major puzzles in solar physics” (Kolotkov, Duckenfield, and Nakariakov 2020). Since the magnetic field plays a major role in upper atmosphere heating, perhaps it must participate in the heating function for the slow waves studied (Duckenfield, Kolotkov, and Nakariakov 2021; Kolotkov, Zavershinskii, and Nakariakov 2021; Kolotkov, Nakariakov, and Fihosy 2023). We choose  $H = H(\rho, T)$  as an approximation, because in a low-beta plasma slow magnetoacoustic waves do not effectively perturb the magnetic field and thus degenerate to acoustic waves.

In an equilibrium state with density  $\rho_0$  and temperature  $T_0$ , the balance between heating and radiative losses is expressed by the equation

$$\rho_0 \Lambda(T_0) - H(\rho_0, T_0) = 0. \tag{5}$$

Density and temperature perturbations lead to local heating and cooling misbalance. Due to the uncertainty of the description, the heating function is sometimes assumed to be constant (Parker 1953; Weymann 1960; Priest 2014), so

$$H = \rho_0 \Lambda(T_0). \quad (6)$$

Krishna Prasad, Banerjee, and Van Doorselaere (2014) and Mandal et al. (2016) used a constant heating function when studying the propagation of slow waves in polar plumes and active region fan loops. Claes and Keppens (2019) and Hermans and Keppens (2021) used a similar approach to the study of condensation processes in the solar corona as the most probable scenario for coronal rain and prominence formation. There is one essential feature in determining the heating function. Usually the energy balance equation is written in terms of the pressure or energy density (De Moortel and Hood 2004; Hermans and Keppens 2021); then the heating function is  $H = \rho_0^2 \Lambda(T_0)$ . We use the energy balance in terms of the temperature.

Speculations why such a choice is possible could be as follows. There are few points of view on the phenomena considered here, which are interpreted as compression waves. One of the alternatives is the assumption that periodically repeating magnetic reconnection processes take place, leading to plasma heating. The choice of the wave nature of the phenomenon does not mean the rejection of heating, but it means that heating is characterized by larger spatio-temporal scales. We consider all possible heating processes to be stationary, on the scales considered.

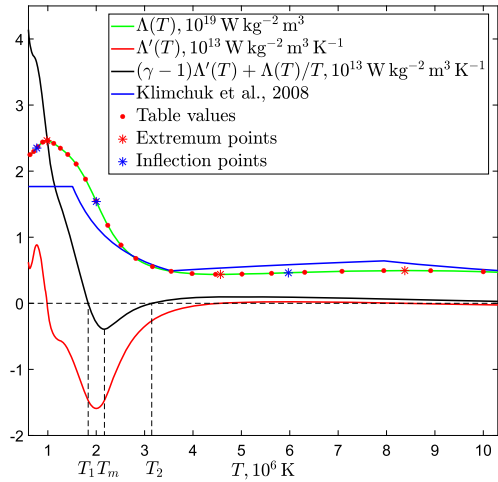
Multiple heating processes in aggregate may create a quasi-steadily heated environment. One potential heating scenario is that the energy release is effectively steady and highly localized at the footpoints of the coronal structures (Lionello et al. 2013). Tripathi, Klimchuk, and Mason (2011) compared the *Hinode/Extreme-Ultraviolet Imaging Spectrometer* (EIS) observations with a simple model of nanoflare-heated loop strands. They firmly believe that the heating is structured on a small scale. If so, direct evidence of nanoflares would be washed out, since the emission from many different strands would be averaged. Hence, steady intensities, densities, Doppler shifts and non-thermal broadening are consistent with both steady heating and nanoflare heating. Orange, Chesny, and Oluseyi (2015), using observations from the *Solar Dynamics Observatory* (SDO)/*Atmospheric Imaging Assembly* (AIA), investigated the dynamics of quiet Sun transients that extrude from a common footpoint shared with heated loop arcades. Quasi-steady interchange reconnection events are implicated as a source of the visibility of the transient bright radiative signature. Also, using observations from the SDO/AIA and the time lag method, Viall and Klimchuk (2016) came to the conclusion that steady emission resulted from steady heating.

The study of wave phenomena can provide information not only on the density and temperature of the plasma, but also on its radiation. It is considered that in this sense, the problem of seismology can be solved with respect to the heating and cooling function form, for example, the heating function, if there is no certainty in its determination (Kolotkov, Duckenfield, and Nakariakov 2020; Kolotkov, Zavershinskii, and Nakariakov 2021). In our case, the radiative intensity and energy inflow are determined independently, and we deal with a given heating and cooling function. In fact, we consider a certain model of heating and radiative loss of the coronal plasma.

### 3. Interpolation of the Radiative-Loss Function

When studying wave processes, it is necessary to have an acceptable analytical representation of the radiative-loss function. To obtain this, we use the cubic spline interpolation

**Figure 1** Interpolation curve of the radiative-loss function  $\Lambda(T)$  (green line) for temperatures from 0.5 to 10 MK. The red dots represent the radiative-loss function values, and the asterisks indicate the radiative-loss function critical points. In the interval  $(T_1, T_2)$ , the instability of acoustic waves is possible.



method. The interpolation procedure is described in detail in Paper I (Derteev et al. 2023). The temperature range is selected from 0.5 to 14 MK. The interpolation is based on 29 tabular values of the coronal plasma emission intensity obtained using the CHIANTI 10 code for a particle density of  $n = 10^{15} \text{ m}^{-3}$ . It will allow us to obtain a smooth analytical expression around any point. For each interval between adjacent points, a polynomial called spline is constructed in such a way that the function and its derivatives are continuous up to the second order on the boundary between adjacent intervals. Thus, interpolation by cubic splines gives us an approximate analytical representation of the function  $\Lambda(T)$  with continuous first and second derivatives. Tabular values are determined for the coefficients of interpolation polynomials, and the values of the function  $\Lambda(T)$  can be found for any temperature from the considered range.

The result is shown in Figure 1, where tabulated temperature values of the radiative-loss function are shown as red dots. For comparison, the approximation from Klimchuk, Patsourakos, and Cargill (2008) is also shown here.

Figure 1 shows the function  $\Lambda(T)$  (green line) in a conventional linear scale. In the interval under consideration, the radiative-loss function has two maxima and one minimum; they are indicated in Figure 1 by red stars. We present them along with other important points: max1 (0.982 MK,  $2.46 \cdot 10^{19} \text{ W kg}^{-2} \text{ m}^3$ ), min (4.57 MK,  $0.428 \cdot 10^{19} \text{ W kg}^{-2} \text{ m}^3$ ), and max2 (8.38 MK,  $0.495 \cdot 10^{19} \text{ W kg}^{-2} \text{ m}^3$ ). All values are given with three significant figures. At the inflection points marked with blue stars, the derivative of the function  $\Lambda'(T)$  (red line) has a local extremum: inf1 (0.771 MK,  $2.35 \cdot 10^{13} \text{ W kg}^{-2} \text{ m}^3 \text{ K}^{-1}$ ), inf2 (2.00 MK,  $1.54 \cdot 10^{13} \text{ W kg}^{-2} \text{ m}^3 \text{ K}^{-1}$ ), and inf3 (5.97 MK,  $0.461 \cdot 10^{13} \text{ W kg}^{-2} \text{ m}^3 \text{ K}^{-1}$ ).

The expression  $(\gamma - 1)\Lambda'(T) + \Lambda(T)/T$  is important when analyzing wave damping and instability (Field 1965; Claes and Keppens 2019; Nakariakov and Kolotkov 2020). It is shown in Figure 1 with a black line. Under the assumption of a constant heating function, instability is possible in a region where it takes negative values. This is shown in Figure 1 in the range  $T_1 < T < T_2$ . Having an expression for the radiative-loss function, we can accurately determine its boundaries:  $T_1 = 1.83 \text{ MK}$ ,  $T_2 = 3.15 \text{ MK}$ . At the minimum point  $T_m = 2.17 \text{ MK}$ , the possibility of instability is the highest, that is,  $(\gamma - 1)\Lambda'(T_m) + \Lambda(T_m)/T_m = -0.392 \cdot 10^{13} \text{ W kg}^{-2} \text{ m}^3 \text{ K}^{-1}$ .

Thus, due to the obtained interpolation of the radiative-loss function, we can indicate the temperature range at which acoustic wave instability can appear.

#### 4. Basic Equations

We consider the plasma as an ideal gas described by

$$p = \rho \frac{RT}{M}, \quad (7)$$

where  $M$  is the mean molar mass,  $M = mN_A$ , where  $m$  is the average mass of a gas particle. For a fully ionized plasma of the solar corona, we define  $m = 0.62m_p \approx 1.037 \cdot 10^{-27}$  kg, so  $M \approx 0.62 \cdot 10^{-3}$  kg mol<sup>-1</sup>. The equilibrium medium is defined by the parameters  $T_0$ ,  $\rho_0$  or  $n_0$ ,  $\rho_0 = mn_0$ . We consider the value  $n_0 \approx 10^{15}$  m<sup>-3</sup> (Reale 2014), which is typical of the main portion of coronal loops, where compression waves are observed (Ofman and Wang 2002; De Moortel and Hood 2003).

Since the magnetic field plays a major role in the dynamics of the coronal plasma, slow waves are more applicable for the interpretation of compression waves. To simplify the problem, we consider the approximation of an infinite medium with a homogeneous magnetic field. For a low- $\beta$  plasma, the slow waves are essentially sound waves, guided by the magnetic field (De Moortel and Hood 2004). We consider the following equations of the gas dynamics:

$$\frac{\partial v_x}{\partial t} + v_x \frac{\partial v_x}{\partial x} = -\frac{R}{M} \frac{\partial T}{\partial x} - \frac{RT}{M\rho} \frac{\partial \rho}{\partial x}, \quad (8)$$

$$\frac{\partial \rho}{\partial t} + \frac{\partial(\rho v_x)}{\partial x} = 0. \quad (9)$$

Let us write the energy balance equation in terms of temperature,

$$\frac{\partial T}{\partial t} + v_x \frac{\partial T}{\partial x} + (\gamma - 1)T \frac{\partial v_x}{\partial x} = -(\gamma - 1) \frac{M}{R} Q, \quad (10)$$

considering the density and temperature as the basic parameters of the plasma. The quantity  $Q$  denotes the amount of energy loss per unit time and per unit mass of gas; its dimension is  $[Q] = \text{W kg}^{-1}$ . We take into consideration only the thermal conductivity and heating and cooling effects in the study of non-adiabatic acoustic waves (Equations 1, 4, and 6). We assume the viscosity and electrical resistance to be insignificant in ordinary coronal conditions:

$$Q = Q_{\text{th}} + Q_{\text{hc}}, \quad (11)$$

$$Q_{\text{th}} = -\frac{1}{\rho} \frac{\partial}{\partial x} \left( \varkappa(T) \frac{\partial T}{\partial x} \right). \quad (12)$$

In a fully ionized high-temperature plasma, heat transfer occurs mainly as a result of electron–electron collisions and subsequent plasma relaxation (Spitzer 1962). In this case, the thermal conductivity is equal to

$$\varkappa = 2.28 \cdot 10^{-11} T^{5/2} \text{ (W m}^{-1} \text{ K}^{-1}\text{)}. \quad (13)$$

In recent years, there have been works indicating that thermal conductivity in a hot plasma may differ from the Spitzer one. In flaring coronal loops, suppression of thermal conductivity and enhancement of compressive viscosity are possible (Wang et al. 2015, 2018; Wang and Ofman 2019; Kolotkov 2022).



It is convenient to determine in advance the scale of the wave parameters based on the characteristic values of the observed phenomena. Let us choose the scales  $m(C_s) = 10^5 \text{ m s}^{-1}$  of an acoustic speed  $C_s = \sqrt{\gamma RT_0/M}$  and frequency  $m(\omega) = 0.1 \text{ s}^{-1}$  as the initial ones. The corresponding value of the oscillation period is  $P = 20\pi \text{ s} \approx 1 \text{ min}$ , which coincides in order of magnitude with the observed periods of compression waves (Srivastava et al. 2008; De Moortel 2009; Banerjee, Gupta, and Teriaca 2011; Krishna Prasad, Banerjee, and Gupta 2011; Wang 2011). The scale of wave number values is set by the relation  $m(\omega) = m(C_s)m(k)$ ;  $m(k) = 10^{-6} \text{ m}^{-1}$ . Dimensionless values are denoted by a ‘‘tilde’’:

$$\tilde{\omega} = m(\omega)^{-1}\omega, \tilde{k} = m(k)^{-1}k, \tilde{C}_s = m(C_s)^{-1}C_s. \tag{14}$$

Let us consider the wave distributions in the form of functions  $\exp(i\tilde{k}\tilde{x} - i\tilde{\omega}\tilde{t})$ , where the spatial and temporal variables are taken on the scales  $m(x) = 10^6 \text{ m}$  and  $m(t) = 10 \text{ s}$ . We write the dispersion relation in the form

$$\tilde{\omega}^3 + iA\tilde{\omega}^2 - \tilde{\omega}\tilde{C}_s^2\tilde{k}^2 + iB = 0, \tag{15}$$

$$A = A_1\tilde{k}^2 + A_2, B = \frac{1}{\gamma} \left( -A_1\tilde{k}^2 - A_2 + A_3 \right) \tilde{C}_s^2\tilde{k}^2. \tag{16}$$

The dimensionless coefficients  $A_1, A_2$  and  $A_3$ , included in the imaginary part of the relation, take a central place in the analysis of the non-adiabatic wave behavior. They are determined by the following expressions:

$$A_1 = \frac{(\gamma - 1)Mm(k)^2}{R\rho_0m(\omega)} \varkappa(T_0), \tag{17}$$

$$A_2 = \frac{(\gamma - 1)M}{Rm(\omega)} \rho_0\Lambda'(T_0), \tag{18}$$

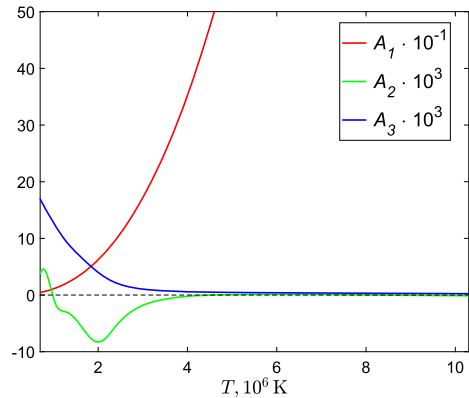
$$A_3 = \frac{(\gamma - 1)M}{RT_0m(\omega)} \rho_0\Lambda(T_0). \tag{19}$$

It should be noted that the coefficient  $A_1$  is determined by the thermal conductivity and the coefficient  $A_2$  is determined by the derivative of the radiative-loss function. In the decay, the interval of the function  $A_2$  takes negative values, which affects the wave stability. The frequency obtained from the dispersion relation (Equation 15) depends not only on the wave number, but also on the basic thermodynamic parameters:  $\tilde{\omega} = \tilde{\omega}(\tilde{k}, T_0, \rho_0)$ . For the non-adiabaticity coefficients  $A_1 = A_2 = A_3 = 0$ , we use the usual non-dissipative acoustic wave  $\tilde{\omega}^2 = \tilde{C}_s^2\tilde{k}^2$ . In the presence of thermal conductivity, the equation has a fourth-order wave number and can be written approximately as  $\tilde{\omega}^2 - \tilde{C}_s^2\tilde{k}^2/\gamma = 0$  in the limit  $\tilde{k} \rightarrow \infty$ . The thermal conduction is supereffective in the dynamics of the acoustic wave for large wave number (Nakariakov and Kolotkov 2020).

Figure 2 shows the temperature dependence of the non-adiabaticity coefficients for a given particle density  $n_0 = 10^{15} \text{ m}^{-3}$ . It is not difficult to obtain these values for another density  $n_0$  referring to Equations 17–19. At high temperatures, the efficiency of the heating and cooling misbalance is low in comparison with the thermal conductivity, regardless of the wave number. This is due to the properties of the heating and cooling function considered here. Obviously, when the density increases, the coefficient  $A_1$  decreases and the coefficients  $A_2$  and  $A_3$  increase in magnitude. Let us recall that the radiative-loss function



**Figure 2** Distributions of dimensionless non-adiabaticity coefficients in the temperature range from 1 to 10 MK.



itself was constructed for  $n_0 = 10^{15} \text{ m}^{-3}$ , so the density changes are possible within limited boundaries. We consider here the limits  $n_0 = (0.5 - 5) \cdot 10^{15} \text{ m}^{-3}$ .

In particular, for  $n_0 = 10^{15} \text{ m}^{-3}$  and  $T_0 = 1.0 \text{ MK}$ , we get  $A_1 = 11.0$ ,  $A_2 = -0.509 \cdot 10^{-3}$ ,  $A_3 = 12.8 \cdot 10^{-3}$ . In the case  $n_0 = 10^{15} \text{ m}^{-3}$  and  $T_0 = 6.3 \text{ MK}$ , the first coefficient exceeds the rest even more:  $A_1 = 1.10 \cdot 10^3$ ,  $A_2 = 0.115 \cdot 10^{-3}$ ,  $A_3 = 0.386 \cdot 10^{-3}$ . It may seem that at the temperature  $T_0 \approx 10 \text{ MK}$  the thermal conductivity effect will be dominant. However, with  $A_1$  increasing, the damping rate due to thermal conductivity tends to zero at non-zero wave numbers. We will show it further. There is a certain temperature limit where the thermal conductivity has no effect on wave damping. We stress that the coefficients at the minimum point of the expression  $(\gamma - 1)\Lambda'(T) + \Lambda(T)/T$ , when  $T_m = 2.17 \text{ MK}$ , are

$$A_1 = 76.4, A_2 = -7.64 \cdot 10^{-3}, A_3 = 3.06 \cdot 10^{-3}. \tag{20}$$

They are especially significant for estimating the acoustic wave instability. Claes and Kepens (2019) found that the slow and fast waves are unstable in a small temperature range near 2 MK. We obtain a similar result for acoustic waves: they are unstable near 2.17 MK in the temperature interval from  $T_1 = 1.83 \text{ MK}$  to  $T_2 = 3.15 \text{ MK}$ .

### 5. Wave Instability

The temporal behavior of waves is determined by the expression

$$e^{-i\tilde{\omega}t} = e^{\text{Im}\tilde{\omega}t} e^{-i\text{Re}\tilde{\omega}t}. \tag{21}$$

If  $\tilde{\delta} = -\text{Im}\tilde{\omega} < 0$ , then acoustic oscillations are stable;  $\tilde{\delta}$  is a damping rate. If  $\tilde{\delta} > 0$ , then an instability occurs, and the relation  $\text{Im}\tilde{\omega}(\tilde{k}, T_0, \rho_0) = 0$  can be considered as the boundary of the wave stability region in the wave number value space and the medium basic parameters. Let us write the dispersion relation on the boundary of the stability region:

$$\begin{aligned} (\text{Re}\tilde{\omega})^3 + i(\text{Re}\tilde{\omega})^2(A_1\tilde{k}^2 + A_2) - \text{Re}\tilde{\omega}\tilde{C}_s^2\tilde{k}^2 - i\frac{1}{\gamma}A_1\tilde{C}_s^2\tilde{k}^4 \\ + i\frac{1}{\gamma}(A_3 - A_2)\tilde{C}_s^2\tilde{k}^2 = 0. \end{aligned} \tag{22}$$

From the real part of the relation for an acoustic wave, we obtain  $\text{Re } \tilde{\omega} = \tilde{C}_s \tilde{k}$ , and we substitute this into the imaginary part. We get the following condition for the wave number:

$$(\gamma - 1)A_1 \tilde{k}^2 + (\gamma - 1)A_2 + A_3 = 0. \tag{23}$$

An instability occurs at

$$(\gamma - 1)A_1 \tilde{k}^2 + (\gamma - 1)A_2 + A_3 < 0. \tag{24}$$

This inequality corresponds to the condition of acoustic wave instability found by Field (1965).

Because  $A_1 \geq 0, A_3 \geq 0$  the occurrence of an instability is possible when

$$(\gamma - 1)A_2 + A_3 \sim (\gamma - 1)\Lambda'(T_0)T_0 + \Lambda(T_0) < 0, \tag{25}$$

if the wave number does not exceed a critical value (Field 1965)

$$\tilde{k}_c = \sqrt{-\frac{(\gamma - 1)A_2 + A_3}{(\gamma - 1)A_1}}. \tag{26}$$

When  $\tilde{k} > \tilde{k}_c$ , the instability is stabilized by the thermal conductivity. If the wavelength of the perturbations exceeds  $\lambda_F = 2\pi/k_c$ , then the plasma should become unstable;  $\lambda_F$  is the Field length (Antolin 2020; Kolotkov, Zavershinskii, and Nakariakov 2021). By analogy with the established terminology for entropy waves, in the application to acoustic waves this variable named the acoustic Field length (Kolotkov, Nakariakov, and Fihosy 2023). The condition in Equation 25 can be written in the following form:

$$-\Lambda'(T_0) > \frac{\Lambda(T_0)}{(\gamma - 1)T_0}. \tag{27}$$

It is similar in form to the Schwarzschild convective instability criterion due to an overadiabatic vertical temperature gradient. In our case, there is an overadiabatic change in the radiative-loss function with temperature.

The instability occurs in the temperature interval from  $T_1 = 1.83$  MK to  $T_2 = 3.15$  MK where  $(\gamma - 1)\Lambda'(T_0) + \Lambda(T_0)/T_0 < 0$  (Figure 1). Obviously, the instability is most pronounced at the minimum point  $T_0 = 2.17$  MK of the expression  $(\gamma - 1)\Lambda'(T_0) + \Lambda(T_0)/T_0$ . In Figure 3 (left)  $\delta = -\text{Im } \omega$  is shown as the wave number function (black line). It takes negative values in the range of small wave numbers; here the wave is unstable. In the absence of thermal conductivity, the wave is unstable at all values of  $k$ , and the thermal conductivity stabilizes it at all  $k$  (red line). The instability is not caused by thermal conductivity, but by heating and cooling misbalance. For  $n_0 = 10^{15} \text{ m}^{-3}$  the non-adiabaticity coefficients take the values from Equation 20. Using them, we can find from Equation 26 the critical wave number  $k_c = 6.3 \cdot 10^{-9} \text{ m}^{-1}$  and estimate the acoustic Field wavelength  $\lambda_F = 10^3$  Mm. This gives a large lower limit for the periods of acoustic oscillations  $P_c = \lambda_F/C_s = 4.6 \cdot 10^3$  s. With the particle density increase, the acoustic Field wavelength and the oscillation period decrease significantly. We obtained  $\lambda_F = 200$  Mm and  $P_c = 0.9 \cdot 10^3$  s for  $n_0 = 5 \cdot 10^{15} \text{ m}^{-3}$ . The value  $\lambda_F = 10^3$  Mm is very large for compressional waves in the coronal loops, but it is of an estimated nature. The same estimated values for the acoustic Field length were obtained in the work of Kolotkov, Nakariakov, and Fihosy (2023). The occurrence of an instability is more realistic at higher densities, for example, for the value  $n_0 = 5 \cdot 10^{15} \text{ m}^{-3}$  and above.

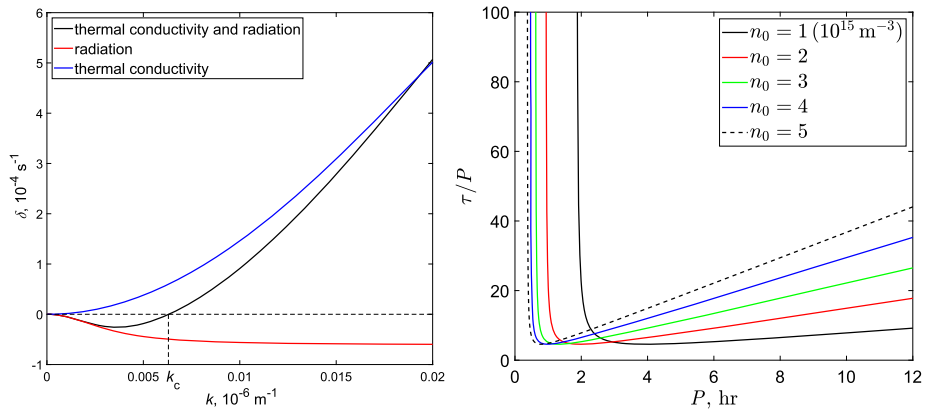


**Figure 3** The coefficient  $\delta = -\text{Im}\omega$ , the wave number function for temperature  $T = 2.17 \text{ MK}$  (left). The wave is unstable for  $0 < k < k_c = 6.3 \cdot 10^{-9} \text{ m}^{-1}$ . It can be seen that the instability is not caused by the thermal conduction, but by heating and cooling misbalance. The relationship between the period of the unstable wave and its growth time for different density values (right).

**Table 1** The shortest time of the instability increase and the corresponding oscillation period at a temperature of  $T_0 = 2.17 \text{ MK}$  for a range of density values.

$n_0, 10^{15} \text{ m}^{-3}$	$P, \text{ h}$	$\tau, \text{ h}$
1	2.97	15.4
2	1.49	7.71
3	0.991	5.14
4	0.743	3.85
5	0.594	3.08

For the density  $n_0 = 10^{15} \text{ m}^{-3}$  the instability growth time is minimal if the period of the oscillations is about 3 h. Figure 3 (right) shows the relationship between the period of unstable oscillations and their growth time at temperature  $T_0 = 2.17 \text{ MK}$ . We consider several density values of the surrounding plasma  $n_0$ ; in each case, we can specify the period with the shortest growth time. The shortest time and the corresponding period are reduced with increasing density (Table 1). Obviously, the shortest growth time indicates the most effective growth of the instability. In the case of  $n_0 = 5 \cdot 10^{15} \text{ m}^{-3}$ , the shortest growth time is  $\tau \approx 3 \text{ h}$  and the period is  $P \approx 0.6 \text{ h}$ . For each individual curve, the relationship between the period and the growth time is a power-law for large periods:

$$\tau/P \sim P, \tau \sim P^2 \text{ at } P \rightarrow \infty. \tag{28}$$

A similar relationship will be discussed in more detail later for damping waves.

## 6. Wave Damping

### 6.1. General Estimate of the Damping

The thermal conduction dominates in the acoustic wave behavior at large wave numbers. With the temperature increase, the coefficient  $A_1$  increases, which determines the thermal

conduction effect, and the coefficients  $A_2$  and  $A_3$  are associated with the decrease in heating and cooling effect (Figure 2). However, this does not mean absolute dominance of the thermal conduction in the wave damping. Indeed, on the one hand, it seems from an asymptotic behavior of the oscillation frequency when  $\tilde{k} \rightarrow \infty$ ,

$$\tilde{\omega} \approx \tilde{v}_\infty \tilde{k} - i \tilde{\delta}_\infty, \quad \tilde{v}_\infty = \tilde{C}_s / \sqrt{\gamma}, \quad \tilde{\delta}_\infty = (\gamma - 1) \tilde{C}_s^2 / (2\gamma A_1), \tag{29}$$

that a limit value of the damping rate due to the thermal conduction does not depend on  $\tilde{k}$  and decreases with increasing thermal conductivity. On the other hand, in the absence of thermal conductivity, the limit values of the phase velocity and the damping rate are equal to

$$\tilde{v}_\infty = \tilde{C}_s, \quad \tilde{\delta}_\infty^{hc} = ((\gamma - 1)A_2 + A_3) / 2\gamma. \tag{30}$$

Here we again see the term  $(\gamma - 1)A_2 + A_3$ , which is responsible for the appearance of the instability of acoustic oscillations. Its positive values characterize the damping rate due to heating and cooling. In Section 4, we noted that the thermal conduction is supereffective for large wave numbers in the sense that the phase speed is isothermal. What can be said about the damping rate? From Equations 29 and 30 we get the ratio

$$\Delta = \frac{\tilde{\delta}_\infty^{hc}}{\tilde{\delta}_\infty^{th}} = \frac{((\gamma - 1)A_2 + A_3)A_1}{(\gamma - 1)\tilde{C}_s^2}. \tag{31}$$

Coefficients of non-adiabaticity are  $A_1 = 11.0$ ,  $A_2 = -0.509 \cdot 10^{-3}$ ,  $A_3 = 12.8 \cdot 10^{-3}$  for  $n_0 = 10^{15} \text{ m}^{-3}$ ,  $T_0 = 1 \text{ MK}$ , and  $A_1 = 3.48 \cdot 10^3$ ,  $A_2 = -0.112 \cdot 10^{-3}$ ,  $A_3 = 0.248 \cdot 10^{-3}$  for  $n_0 = 10^{15} \text{ m}^{-3}$ ,  $T_0 = 10 \text{ MK}$ . We get  $\Delta = 0.093$  and  $\Delta = 0.051$  for  $T_0 = 1 \text{ MK}$  and  $T_0 = 10 \text{ MK}$ , respectively. The limit value of the damping rate due to thermal conduction is equal to  $\tilde{\delta}_\infty^{th} = 0.040$  for  $T_0 = 1 \text{ MK}$  and  $\tilde{\delta}_\infty^{th} = 0.0013$  for  $T_0 = 10 \text{ MK}$ . Indeed, it significantly decreases for high temperatures up to 10 MK, but otherwise the damping rate due to radiation loss and the constant heating function decreases even more strongly. We conclude that at high temperatures within 10 MK, the thermal conduction has a dominant effect on wave damping for large wave numbers. The situation may change at much higher temperatures.

Typical acoustic wave damping is shown in Figure 4 (left column). At  $k \approx 0.5 \cdot 10^{-6} \text{ m}^{-1}$ , the phase speed and damping rate are close to the asymptotic values  $\tilde{v}_\infty^{th} = 1.16$  and  $\tilde{\delta}_\infty^{th} = 0.04$  for  $\tilde{k} \rightarrow \infty$ . The thermal conduction plays the main role in wave damping, but heating and cooling misbalance is noticeable at small wave numbers. Let us find a solution of Equation 15 in the limit  $\tilde{k} \rightarrow 0$ . If  $A_2 < 0$ , we get

$$\tilde{\omega} = \tilde{v}_0 \tilde{k} - i \tilde{\delta}_0, \quad \tilde{v}_0 \approx \sqrt{\frac{A_2 - A_3}{\gamma A_2}} \tilde{C}_s, \quad \tilde{\delta}_0 \approx \frac{(\gamma - 1)A_2 + A_3}{2\gamma A_2^2} \tilde{C}_s^2 \tilde{k}^2, \quad \tilde{k} \rightarrow 0. \tag{32}$$

At  $(\gamma - 1)A_2 + A_3 < 0$ , the wave is unstable; then Equation 28 follows from Equation 32.

For selected  $T_0 = 1 \text{ MK}$  and  $n_0 = 10^{15} \text{ m}^{-3}$ , the limit phase speed is equal to  $\tilde{v}_0 = 5.96$ . We found the numeric values of wave parameters mentioned above using the coefficients  $A_1 = 11.0$ ,  $A_2 = -0.509 \cdot 10^{-3}$  and  $A_3 = 12.8 \cdot 10^{-3}$ . According to Equations 19–21, the non-adiabaticity coefficients depend significantly on the plasma density. For  $T_0 = 1 \text{ MK}$  and  $n_0 = 5 \cdot 10^{15} \text{ m}^{-3}$ , they are  $A_1 = 2.20$ ,  $A_2 = -2.55 \cdot 10^{-3}$  and  $A_3 = 6.40 \cdot 10^{-2}$ . In Figure 5 (left) we show the corresponding phase speed and damping rate. It seems that the heating and cooling misbalance is effective at  $k < 0.2 \cdot 10^{-6} \text{ m}^{-1}$ , corresponding to wavelengths of more than 36 Mm and oscillation periods of more than 5 min.

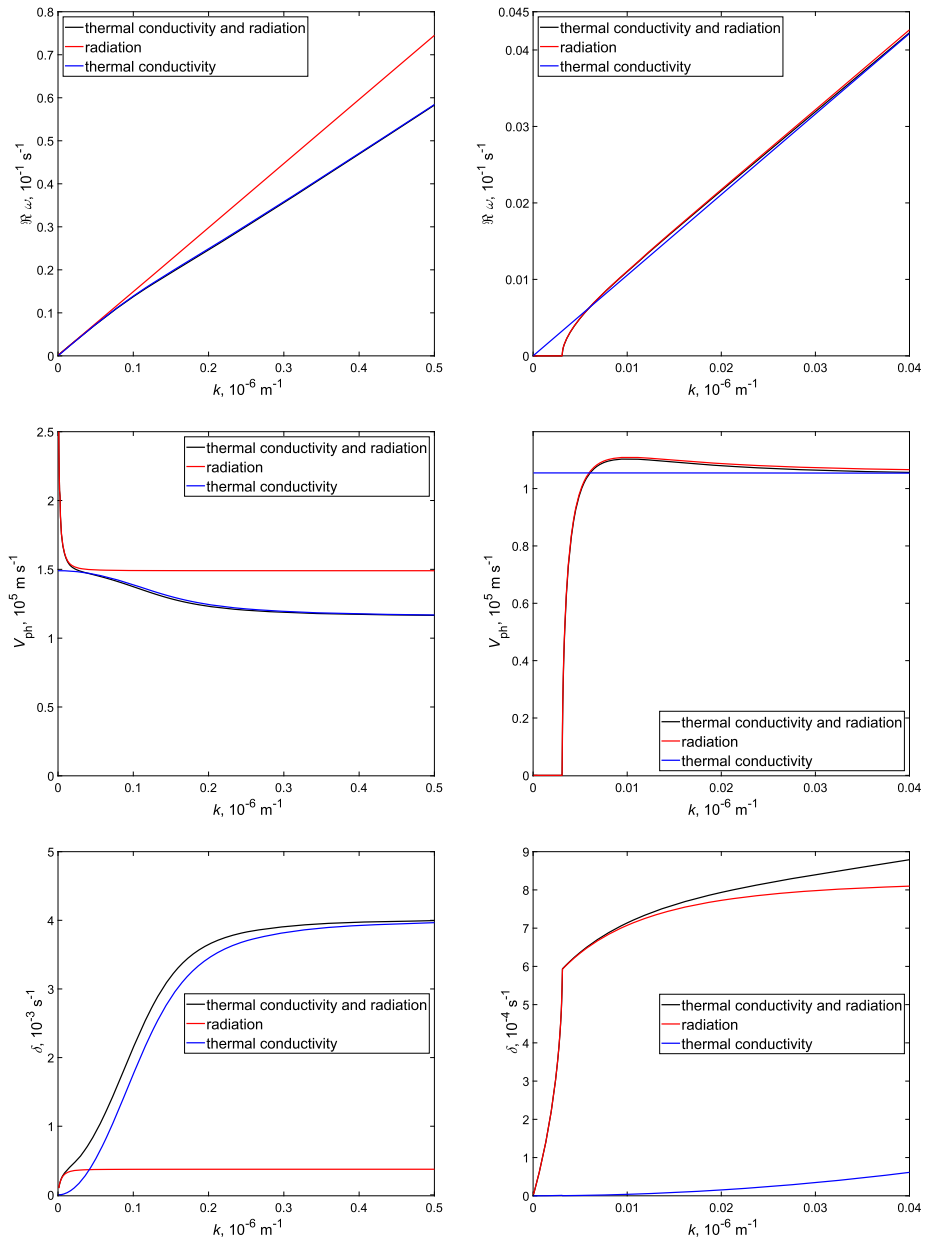


**Figure 4** Dispersion curves and a damping rate for  $T_0 = 1$  MK (left column) and  $T_0 = 0.5$  MK (right column),  $n_0 = 10^{15} \text{ m}^{-3}$ .

Comparing with Figure 4 (left column), one can see that the range of wave numbers where the heating and cooling misbalance becomes effective has significantly expanded. For example, at  $k = 0.2 \cdot 10^{-6} \text{ m}^{-1}$  damping rate values are equal due to both heating and cooling and thermal conduction if  $n_0 = 5 \cdot 10^{15} \text{ m}^{-3}$ . In the case  $n_0 = 10^{15} \text{ m}^{-3}$ , the damping

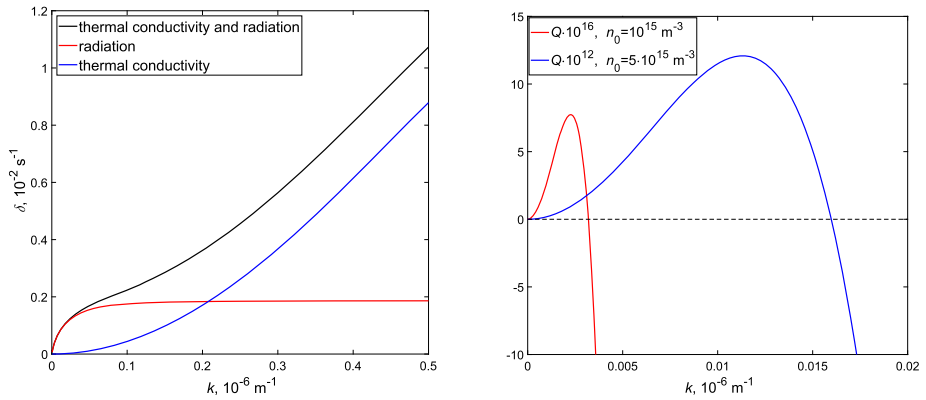


**Figure 5** Damping rate in the case  $T_0 = 1$  MK,  $n_0 = 5 \cdot 10^{15} \text{ m}^{-3}$  (left). Discriminant  $Q$  of equation (15) for  $T_0 = 0.5$  MK,  $n_0 = 10^{15} \text{ m}^{-3}$  and  $n_0 = 5 \cdot 10^{15} \text{ m}^{-3}$  (right).

rate due to thermal conduction is an order of magnitude higher than that due to the heating and cooling misbalance. We can state that the observed fast damping of compression waves (De Moortel and Hood 2004) can be caused by heating and cooling along with thermal conduction assuming a slightly higher plasma density.

The solution shown in Equation 32 is available if  $A_2 < 0$ , i.e. in a temperature range where  $\Lambda(T)$  decreases,  $\Lambda'(T) < 0$ . For the CHIANTI function, we consider that  $0.982 \text{ MK} < T_0 < 4.57 \text{ MK}$  and  $8.38 \text{ MK} < T_0 < 14.1 \text{ MK}$ . In the remaining ranges  $\Lambda(T)$  increases and  $A_2 > 0$ . Here the behavior of the wave is different.

### 6.2. Non-Propagating Waves

The propagation properties of acoustic waves depend on the discriminant  $Q$  of Equation 15 (Zavershinskii et al. 2021):

$$Q = p^3/27 - q^2/4, \tag{33}$$

$$p = a^2/3 - b, \quad q = 2a^3/27 - ab/3 + c, \tag{34}$$

$$a = A_1 \tilde{k}^2 + A_2, \quad b = \tilde{C}_s^2 \tilde{k}^2, \quad c = (A_1 \tilde{k}^2 + A_2 - A_3) \tilde{C}_s^2 \tilde{k}^2 / \gamma. \tag{35}$$

For all parameters,  $Q$  takes real values. An acoustic wave is propagating if  $Q < 0$  and non-propagating if  $Q > 0$ . For a given temperature and density, we consider  $Q$  as a function of the wave number. The separating wave number  $k_0$  is determined from the equation  $Q(k_0) = 0$ . In Figure 5 (right), it is shown for  $T_0 = 0.5$  MK,  $n_0 = 10^{15} \text{ m}^{-3}$  and  $n_0 = 5 \cdot 10^{15} \text{ m}^{-3}$ .

Dispersion curves and the damping rate for  $T_0 = 0.5$  MK are given in Figure 4 (right column). The first thing to pay attention to is the lack of oscillations for  $k < k_0 = 3.2 \cdot 10^{-9} \text{ m}^{-1}$  if  $n_0 = 10^{15} \text{ m}^{-3}$ . The wave is non-propagating in this case, and the frequency is purely imaginary,  $\omega = -i\delta$ ,  $\delta > 0$ . In this case, we obtain a more critical value of the wave number separating region for the non-propagating one. The corresponding damping rate value is  $\delta_0 = 6 \cdot 10^{-4} \text{ s}^{-1}$ , i.e. the damping time is  $\tau_0 = 1/\delta_0 = 1670 \text{ s}$ . For  $n_0 = 5 \cdot 10^{15} \text{ m}^{-3}$  we get  $k_0 = 0.016 \cdot 10^{-6} \text{ m}^{-1}$ ,  $\lambda_0 = 400 \text{ Mm}$ ,  $\delta_0 = 3 \cdot 10^{-3} \text{ s}^{-1}$  and  $\tau_0 = 330 \text{ s}$ . With the increase of density, the wave parameters change greatly and the non-propagating

**Table 2** Parameters of compressive waves in hot coronal loops (Wang, Innes, and Qiu 2007).

Loop	$L$ (Mm)	$T$ (MK)	$n_e$ ( $10^9 \text{ cm}^{-3}$ )	$v$ ( $\text{km s}^{-1}$ )	$P$ (min)	$\tau$ (min)
1	134	$6.6 \pm 0.1$	$5.2 \pm 0.1$	21	$12.9 \pm 0.2$	$18.1 \pm 3.1$
2	275	$6.5 \pm 0.3$	$4.3 \pm 0.5$	36	$18.3 \pm 0.7$	$19.9 \pm 4.2$
3	92	$7.0 \pm 0.3$	$14.1 \pm 0.8$	14	$8.1 \pm 0.1$	$19.8 \pm 5.0$
4	74	$6.4 \pm 0.9$	$10.4 \pm 2.0$	17	$8.5 \pm 0.2$	$7.4 \pm 1.7$
5	98	$6.3 \pm 0.9$	$11.1 \pm 2.3$	8	$9.3 \pm 0.3$	$19.1 \pm 9.2$
6	82	$6.3 \pm 0.5$	$7.8 \pm 0.9$	30	$8.1 \pm 0.3$	$7.2 \pm 1.8$
7	135	$5.9 \pm 0.3$	$5.6 \pm 0.5$	61	$13.3 \pm 0.7$	$8.1 \pm 2.3$

wave becomes real. The oscillations occur in the absence of heating and cooling; therefore, a non-propagating wave is caused by heating and cooling misbalance. Zavershinskii et al. (2021) got a similar result. They used a more general expression for the heating and cooling function and set conditions for non-propagating waves in terms of characteristic misbalance times. Our specific heating and cooling function allows to express these conditions in terms of wave parameters and the basic physical plasma parameters.

### 6.3. Waves in Hot Coronal Loops

It remains to consider the temperature range from 4.57 to 8.38 MK, where compression waves are observed in hot coronal loops. The radiative-loss function increases in this range. Similarly to the region from 0.5 to 0.982 MK with derivative  $\Lambda'(T) > 0$ , non-propagating waves may appear here. For  $T_0 = 6.31$  MK and  $n_0 = 5 \cdot 10^{15} \text{ m}^{-3}$ , they can exist if  $k_0 < 4.2 \cdot 10^{-11} \text{ m}^{-1}$  or  $\lambda_0 > 1.5 \cdot 10^5$  Mm. The critical wavelength value  $\lambda_0$  is one order of magnitude larger if  $n_0 = 5 \cdot 10^{15} \text{ m}^{-3}$ . It is safe to assume that there are no non-propagating waves in hot coronal loops.

There are *Solar Ultraviolet Measurements of Emitted Radiation* (SUMER) observations of a fast damping of longitudinal waves in hot coronal loops which are consistent with standing slow waves in their fundamental mode (Wang 2007; Wang 2011). The average values of oscillation parameters are: oscillation period,  $17.6 \pm 5.4$  min; damping time,  $14.6 \pm 7.0$  min; amplitude,  $98 \pm 75 \text{ km s}^{-1}$ . Data related to longitudinal oscillations of seven individual coronal loops are presented in the article of Wang, Innes, and Qiu (2007); these data are shown in Table 2. It should be noted that at the temperatures presented here, the speed of sound is  $C_s = 365 - 395 \text{ km s}^{-1}$ . With the exception of loop 7, the speeds do not exceed 10% of the sound speed; therefore, with some accuracy, a linear approach is applicable to the oscillations under consideration.

On the basis of data about the loop sizes, temperature and particle density, we calculated the oscillation period and damping time using the current model. The calculation results are shown in Table 3. In general, they can be considered close to the observational data, taking into account the large empirical error in finding the damping time. There is more similarity in the values of the periods. The similarity is greater for shorter loops, and the discrepancy between the empirical and theoretical results for loops 2 and 3, which have the largest geometric dimensions, is striking. The discrepancy can also be explained by the non-linearity of the oscillations, since in most cases they cannot be considered as small.

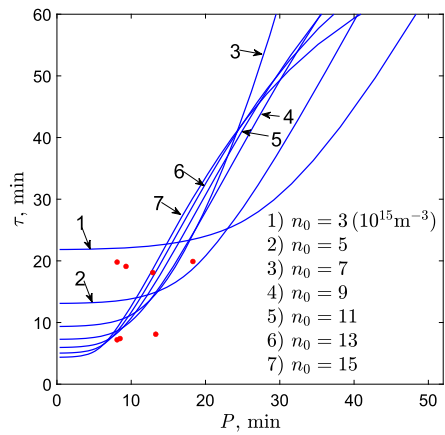
Table 3 presents the results of calculations separately for each of the two non-adiabatic effects: thermal conductivity, and heating and cooling. In all cases, the damping time is



**Table 3** Period and damping time of compressive oscillations in hot coronal loops obtained from our model in the linear approximation. *th*, effect of the thermal conductivity; *hc*, effect of the heating and cooling imbalance; *th, hc*, effect of both mechanisms.

Loop	$P_{th}$ (min)	$\tau_{th}$ (min)	$P_{hc}$ (min)	$\tau_{hc}$ (min)	$P_{th,hc}$ (min)	$\tau_{th,hc}$ (min)
1	13.7	15.0	11.7	240	13.8	14.5
2	26.0	32.2	24.2	290	26.2	29.3
3	8.4	10.3	7.8	109	8.4	9.4
4	7.6	8.2	6.5	120	7.6	7.9
5	9.5	11.2	8.7	113	9.6	10.4
6	8.7	9.9	7.3	160	8.7	9.6
7	14.1	15.3	12.4	216	14.2	14.6

**Figure 6** The relationship between the period and the damping time of acoustic waves in a hot coronal plasma,  $T_0 = 6.3$  MK. Red circles show the damping oscillations presented in Table 2.



long due to the possible single effect of heating and cooling imbalance. At high temperatures, its role turns out to be insignificant for the considered wavelengths. For very large wavelengths, i.e. near zero on the wave number axis, there is a non-propagating wave, i.e. theoretically, one can find situations where heating and cooling imbalance can exist even at high temperatures. This result is derived under the assumption of a constant heating function. For non-constant heating functions, heating and cooling imbalance may have a significant impact on acoustic wave damping (Kolotkov, Nakariakov, and Zavershinskii 2019; Duckenfield, Kolotkov, and Nakariakov 2021). It is also necessary to recall the effect of suppression of thermal conductivity in flaring loops (Wang et al. 2015, 2018; Wang and Ofman 2019).

At a given density and temperature, from the dispersion relation, a relationship between the damping time and the oscillation period can be established. A similar relationship for the growth time is shown in Figure 4 (right) for unstable waves and in Figure 6 for the damping time. For each pair  $n_0$  and  $T_0$  there is a certain damping time curve  $\tau(P)$ . For comparison, the parameters of damped oscillations in hot coronal loops presented in Table 2 are shown (red circles). In analogy, the scaling of the damping time with the oscillation period of a slow mode for various temperatures was studied (Nakariakov et al. 2019). We take a number of density values for  $T_0 = 6.3$  MK. This point lies in the temperature interval where acoustic waves are non-propagating. Equation 32 is not valid here. The damping rate curve in Figure 4 (right column) shows that  $\tau$  increases infinitely with increasing  $P$ . According to Equation 29,  $\tau$  has a non-zero constant limit at  $P \rightarrow 0$ .

It follows from Figure 6 that damping time curves  $\tau(P)$  fill a certain area on a plane  $(P, \tau)$ . This turns out to be because in addition to temperature, the plasma has another parameter, namely, density. In our model, the density  $n_0$  and temperature  $T_0$  are input parameters, and the period  $P$  and damping time  $\tau$  are output parameters. Because of various values of  $n_0$  and  $T_0$ , a function  $\tau(P, n_0, T_0)$  gives a set of points in some areas. A functional dependency can be established for some subsets. A distribution of an entire set of points is generally statistical in nature.

The next step in the study may be the consideration of non-linear oscillations, for which a numerical experiment is usually carried out. In this article, we considered longitudinal standing oscillations in hot coronal loops as a practical application of the model. As is well known, there are observations of compressive waves, including traveling waves, in other coronal structures.

## 7. Discussion

For a number of values of the radiative-loss function found using CHIANTI 10 code, we built its approximate analytical representation in the form of cubic splines. The CHIANTI radiative-loss function  $\Lambda(T)$  was used in the study of slow waves in the solar corona (Kolotkov, Nakariakov, and Zavershinskii 2019; Kolotkov, Duckenfield, and Nakariakov 2020; Duckenfield, Kolotkov and Nakariakov 2021; Kolotkov, Zavershinskii and Nakariakov 2021). We present an explicit and sufficiently accurate method to calculate values of  $\Lambda(T)$  and its derivative for any  $T$ . In combination with the generally accepted thermal conductivity (Spitzer 1962), it gives us a specific model of acoustic oscillations for the description of coronal compression waves. The choice of a constant heating function leads to a model limitation, but it is common not only due to ignorance of the heating mechanisms in specific situations. The concept of nanoflares makes it possible to imagine that the foot-points of coronal loops are continuously heated due to the energy inflow from the dense atmosphere layers (Warren, Winebarger, and Brooks 2010; Viall and Klimchuk 2016). It should be noted that we used the energy inflow per time unit per mass unit of the plasma; often a volume unit is considered instead (De Moortel and Hood 2004; Hermans and Keppens 2021). The model obtained in this way can be used to diagnose the coronal plasma because it allows to directly find specific values of the main physical coronal plasma parameters, namely, density and temperature. The current model can be further refined and developed by introducing a non-constant heating function. We plan to devote a series of articles to this problem; in this article we have tried to evaluate the role of both non-adiabatic effects, i.e. thermal conductivity and heating and cooling, in the behavior of acoustic waves.

The dispersion relation analysis shows that over a significant range of wave number values, thermal conductivity plays a decisive role in the damping of acoustic waves. The misbalance between heating and cooling can compete with thermal conductivity only at wavelengths of more than 30 Mm for a temperature of 1 MK and 300 Mm for a temperature of 6.3 MK. This is consistent with typical wavelengths of observed compression waves in warm and hot coronal loops: 20–100 Mm (De Moortel and Hood 2004; De Moortel 2009) and a few hundred Mm (Ofman and Wang 2002; Wang, Innes, and Qiu 2007; Wang 2011), respectively. We can state that a slightly higher plasma density can lead to fast damping of acoustic waves due to heating and cooling misbalance. This means that the observed fast damping of compression waves (De Moortel and Hood 2004) can be explained by heating and cooling effects along with the thermal conduction. The described model of non-adiabatic acoustic

waves is applied to standing waves in hot coronal loops. The performed theoretical calculations are in good agreement with the observational data presented in the work of Wang, Innes, and Qiu (2007).

It is known from a general theory (Field 1965) that acoustic waves can be unstable at the temperature value at which the radiative-loss function decreases. Claes and Keppens (2019) found that the slow and fast waves in the corona are unstable in a small range at approximately 2 MK. We obtained a similar result for acoustic waves, which are most likely to be unstable close to 2.2 MK. The period and growth time are around 1 h and decrease with increasing plasma density. The acoustic Field length changes from 1000 Mm to 200 Mm when the plasma density varies from  $10^{-12}$  kg m $^{-3}$  to  $5 \cdot 10^{-12}$  kg m $^{-3}$ . The instability of coronal loops can be real at a sufficiently high density. The whole theoretical range of the instability of acoustic waves extends from  $T_1 = 1.8$  to  $T_2 = 3.2$  MK. The waves described here belong to the ranges  $0.98 \text{ MK} < T < 4.6 \text{ MK}$  and  $T > 8.4 \text{ MK}$ , where  $\Lambda'(T) < 0$ . They are damping and unstable propagating waves. In ranges where  $\Lambda'(T) > 0$  there are damping propagating and non-propagating waves. Zavershinskii et al. (2021) found conditions of non-propagating waves in terms of characteristic misbalance times. We determined these conditions in terms of physical parameters, namely, density and temperature. Non-propagating waves may appear in the ranges of  $0.5 \text{ MK} < T < 0.98 \text{ MK}$  and  $4.6 \text{ MK} < T < 8.4 \text{ MK}$ . Additionally, the density determines corresponding wavelength ranges. We got  $\lambda > 1900 \text{ Mm}$  at  $n = 10^{15} \text{ m}^{-3}$  and  $\lambda > 400 \text{ Mm}$  at  $n = 5 \cdot 10^{15} \text{ m}^{-3}$  for the same temperature  $T = 0.5 \text{ MK}$ . We got a real non-propagating wave at higher densities. The fast damping of compression waves in warm and hot coronal loops can be explained by acoustic oscillations in a dense plasma. Unstable and non-propagating acoustic waves can really exist under the assumption of a sufficiently high plasma density. That means that the heating and cooling effect is significant at high densities. Therefore, linking the wave properties with physical parameters of the plasma, we formed a basis for plasma diagnostics with the help of coronal seismology by non-adiabatic acoustic waves, where the heating and cooling misbalance plays a significant role.

**Acknowledgments** The authors would like to thank the journal editors and anonymous reviewers for useful comments.

**Author contributions** B. Mikhalyaev wrote the main manuscript text, M. Sapraliev, S. Derteev, N. Shividov and D. Bembitov prepared figures. All authors reviewed the manuscript.

**Funding** This work was supported by the Ministry of Science and Higher Education of the Russian Federation, grant number 075-03-2022-119/1 (Development of new observational and theoretical approaches in space weather forecasting based on ground-based observations).

**Data Availability** All the data used in this study (SUMER) are publicly available.

## Declarations

**Competing interests** The authors declare no competing interests.

## References

- Antolin, P.: 2020, Thermal instability and non-equilibrium in solar coronal loops: from coronal rain to long-period intensity pulsations. *Plasma Phys. Control. Fusion* **62**, 014016. DOI.
- Aschwanden, M.J., Terradas, J.: 2008, The effect of radiative cooling on coronal loop oscillations. *Astrophys. J.* **686**, L127. DOI.

- Banerjee, D., Gupta, G.R., Teriaca, L.: 2011, Propagating MHD waves in coronal holes. *Space Sci. Rev.* **158**, 267. DOI.
- Banerjee, D., Krishna Prasad, S.: 2016, MHD waves in coronal holes. In: *Low-Frequency Waves in Space Plasmas, Geophys. Monogr. Ser.* **216**, Wiley, US 419. DOI.
- Belov, S.A., Molevich, N.E., Zavershinskii, D.L.: 2021, Dispersion of slow magnetoacoustic waves in the active region fan loops introduced by thermal misbalance. *Solar Phys.* **296**, 122. DOI.
- Carbonell, M., Oliver, R., Ballester, J.L.: 2004, Time damping of linear non-adiabatic magnetohydrodynamic waves in an unbounded plasma with solar coronal properties. *Astron. Astrophys.* **415**, 739. DOI.
- Claes, N., Keppens, R.: 2019, Thermal stability of magnetohydrodynamic modes in homogeneous plasmas. *Astron. Astrophys.* **624**, A96. DOI.
- De Moortel, I.: 2009, Longitudinal waves in coronal loops. *Space Sci. Rev.* **149**, 65. DOI.
- De Moortel, I., Browning, P.: 2015, Recent advances in coronal heating. *Phil. Trans. R. Acad. Sci. A* **373**, 20140269. DOI.
- De Moortel, I., Hood, A.W.: 2003, The damping of slow MHD waves in solar coronal magnetic fields. *Astron. Astrophys.* **408**, 755. DOI.
- De Moortel, I., Hood, A.W.: 2004, The damping of slow MHD waves in solar coronal magnetic fields II. The effect of gravitational stratification and field line divergence. *Astron. Astrophys.* **415**, 705. DOI.
- De Moortel, I., Nakariakov, V.M.: 2012, Magnetohydrodynamic waves and coronal seismology: an overview of recent results. *Phil. Trans. Roy. Soc. A* **370**, 3193. DOI.
- Del Zanna, G., Dere, K.P., Young, P.R., Landi, E.: 2021, CHIANTI – an atomic database for emission lines. XVI. Version 10, further extensions. *Astrophys. J.* **909**, 38. DOI.
- Dere, K.P., Landi, E., Mason, H.E., Monsignori Fossi, B.C., Young, P.R.: 1997, CHIANTI – an atomic database for emission lines. *Astron. Astrophys. Suppl. Ser.* **125**, 149. DOI.
- Dere, K.P., Landi, E., Young, P.R., Del Zanna, G., Landini, M., Mason, H.E.: 2009, CHIANTI – an atomic database for emission lines IX. Ionization rates, recombination rates, ionization equilibria for the elements hydrogen through zinc and updated atomic data. *Astron. Astrophys.* **498**, 915. DOI.
- Derteev, S.B., Shvidov, N.K., Bembitov, D.B., Mikhalyaev, B.B.: 2023, Damping and dispersion of non-adiabatic acoustic waves in a high-temperature plasma: a radiative-loss function. *Physics* **5**, 215. DOI.
- Duckenfield, T.J., Kolotkov, D.Y., Nakariakov, V.M.: 2021, The effect of the magnetic field on the damping of slow waves in the solar corona. *Astron. Astrophys.* **646**, A155. DOI.
- Dudík, J., Dzifčáková, E., Karlický, M., Kulinová, A.: 2011, The bound-bound and free-free radiative losses for the nonthermal distributions in solar and stellar coronae. *Astron. Astrophys.* **529**, A103. DOI.
- Erdélyi, R., Ballai, I.: 2007, Heating of the solar and stellar coronae: a review. *Astron. Nachr.* **8**, 726. DOI.
- Field, G.B.: 1965, Thermal instability. *Astrophys. J.* **142**, 531. DOI.
- Hermans, J., Keppens, R.: 2021, Effect of optically thin cooling curves on condensation formation: case study using thermal instability. *Astron. Astrophys.* **635**, A36. DOI.
- Hildner, E.: 1974, The formation of solar quiescent prominences by condensation. *Solar Phys.* **35**, 123. DOI.
- Ibanez, M.H., Ballester, J.L.: 2022, The effect of thermal misbalance on slow magnetoacoustic waves in a partially ionized prominence-like plasma. *Solar Phys.* **297**, 144. DOI.
- Klimchuk, J.A.: 2015, Key aspects of coronal heating. *Phil. Trans. R. Acad. Sci. A* **373**, 20140256. DOI.
- Klimchuk, J.A., Patsourakos, S., Cargill, P.J.: 2008, Highly efficient modeling of dynamic coronal loops. *Astrophys. J.* **682**, 1351. DOI.
- Kolotkov, D.Y.: 2022, Coronal seismology by slow waves in non-adiabatic conditions. *Front. Astron. Space Sci.* **9**, 1073664. DOI.
- Kolotkov, D.Y., Duckenfield, T.J., Nakariakov, V.M.: 2020, Seismological constraints on the solar coronal heating function. *Astron. Astrophys.* **644**, A33. DOI.
- Kolotkov, D.Y., Nakariakov, V.M., Fihosy, J.B.: 2023, Stability of slow magnetoacoustic and entropy waves in the solar coronal plasma with thermal misbalance. *Physics* **5**, 193. DOI.
- Kolotkov, D.Y., Nakariakov, V.M., Zavershinskii, D.I.: 2019, Damping of slow magnetoacoustic oscillations by the misbalance between heating and cooling processes in the solar corona. *Astron. Astrophys.* **626**, A133. DOI.
- Kolotkov, D.Y., Zavershinskii, D.I., Nakariakov, V.M.: 2021, The solar corona as an active medium for magnetoacoustic waves. *Plasma Phys. Control. Fusion* **63**, 124008. DOI.
- Krishna Prasad, S., Banerjee, D., Gupta, G.R.: 2011, Propagating intensity disturbances in polar corona as seen from AIA/SDO. *Astron. Astrophys.* **528**, L4. DOI.
- Krishna Prasad, S., Banerjee, D., Van Doorselaere, T.: 2014, Frequency-dependent in propagating slow magneto-acoustic waves. *Astrophys. J.* **789**, 118. DOI.
- Krishna Prasad, S., Van Doorselaere, T.: 2021, Compressive oscillations in hot coronal loops: are sloshing oscillations and standing slow waves independent? *Astron. Astrophys.* **914**, 81. DOI.
- Kumar, S., Nakariakov, V.M., Moon, Y.-J.: 2016, Effect of a radiation cooling and heating function on standing longitudinal oscillations in coronal loops. *Astrophys. J.* **824**, 8. DOI.

- Landi, E., Landini, M., Dere, K.P., Young, P.R., Mason, H.E.: 1999, CHIANTI – an atomic database for emission lines III. Continuum radiation and extension of the ion database. *Astron. Astrophys. Suppl. Ser.* **135**, 339. DOI.
- Lionello, R., Winebarger, A.R., Mok, Y., Linker, J.A., Mikić, Z.: 2013, Thermal non-equilibrium revisited: a heating model for coronal loops. *Astrophys. J.* **773**, 134. DOI.
- Mandal, S., Magyar, N., Yuan, D., Van Doorselaere, T., Banerjee, D.: 2016, Forward modeling of propagating slow waves in coronal loops and their frequency-dependent damping. *Astrophys. J.* **820**, 13. DOI.
- Mikhalyaev, B.B., Veselovskii, I.S., Khongorova, O.V.: 2013, Radiation effects on the MHD wave behavior in the solar corona. *Solar Syst. Res.* **47**, 50. DOI.
- Nakariakov, V.M., Kolotkov, D.Y.: 2020, Magnetohydrodynamic waves in the solar corona. *Annu. Rev. Astron. Astrophys.* **58**, 441. DOI.
- Nakariakov, V.M., Kosak, M.K., Kolotkov, D.Y., Anfinogentov, S.A., Kumar, P., Moon, Y.-J.: 2019, Properties of slow magnetoacoustic oscillations of solar coronal loops by multi-instrumental observations. *Astrophys. J. Lett.* **874**, L1. DOI.
- Narain, U., Ulmschneider, P.: 1996, Chromospheric and coronal heating mechanisms. II. *Space Sci. Rev.* **75**, 453. DOI.
- Ofman, L., Wang, T.: 2002, Hot coronal loop oscillations observed by SUMER: slow magnetosonic wave damping by thermal conduction. *Astrophys. J.* **580**, L85. DOI.
- Orange, N.B., Chesny, D.L., Olusey, H.M.: 2015, Observations of an energetically isolated quiet Sun transient: evidence of quasi-steady coronal heating. *Astrophys. J.* **810**, 98. DOI.
- Parker, E.N.: 1953, Instability of thermal fields. *Astrophys. J.* **117**, 431. DOI.
- Prasad, A., Srivastava, A.K., Wang, T.: 2021, Role of compressive viscosity and thermal conductivity on the damping of slow Waves in coronal loops with and without heating-cooling imbalance. *Solar Phys.* **296**, 1. DOI.
- Priest, E.R.: 2014, *Magnetohydrodynamics of the Sun*, Cambridge University Press, Cambridge, 576. DOI.
- Priest, E.R., Foley, C.R., Heyvaerts, J., Arber, T.D., Culhane, J.L., Acton, L.W.: 1998, Nature of the heating mechanism for the diffuse solar corona. *Nature* **393**, 545. DOI.
- Reale, F.: 2014, Coronal loops: observations and modeling of confined plasma. *Living Rev. Solar Phys.* **11**, 4. DOI.
- Rosner, R., Tucker, W.H., Vaiana, G.S.: 1978, Dynamics of the quiescent solar corona. *Astrophys. J.* **220**, 643. DOI.
- Soler, R., Ballester, J.L., Goossens, M.: 2011, The thermal instability of solar prominence threads. *Astrophys. J.* **731**, 39. DOI.
- Somov, B.V., Syrovatskij, S.I.: 1980, Thermal instability of a current sheet as the origin of the cool coronal loops. *Sov. Astron. Lett.* **6**, 310. ADS.
- Spitzer, L.J.: 1962, *Physics of Fully Ionized Gases*, Wiley, NY, 170.
- Srivastava, A.K., Kuridze, D., Zaqarashvili, T.V., Dwivedi, B.N.: 2008, Intensity oscillations observed with Hinode near the south pole of the Sun: leakage of low frequency magneto-acoustic waves into the solar corona. *Astron. Astrophys.* **481**, L95. DOI.
- Taroyan, Y., Erdélyi, R.: 2009, Heating diagnostics with MHD waves. *Space Sci. Rev.* **149**, 229. DOI.
- Tripathi, D., Klimchuk, J.A., Mason, H.E.: 2011, Emission measure distribution and heating of two active region cores. *Astrophys. J.* **740**, 111. DOI.
- Viall, N.M., Klimchuk, J.A.: 2016, Signatures of steady heating in time lag analysis of coronal emission. *Astrophys. J.* **828**, 76. DOI.
- Wang, T.: 2011, Standing slow-mode waves in hot coronal loops: observations, modeling, and coronal seismology. *Space Sci. Rev.* **158**, 397. DOI.
- Wang, T.: 2016, Waves in solar coronal loops. In: *Low-Frequency Waves in Space Plasmas, Geophys. Monogr. Ser.* **216**, Wiley, US 395. DOI.
- Wang, T., Innes, D.E., Qiu, J.: 2007, Determination of the coronal magnetic field from hot-loop oscillations observed by SUMER and SXT. *Astrophys. J.* **656**, 598. DOI.
- Wang, T., Ofman, O.: 2019, Determination of transport coefficients by coronal seismology of flare-induced slow-mode waves: numerical parametric study of a 1D loop model. *Astrophys. J.* **886**, 2. DOI.
- Wang, T., Ofman, O., Sun, X., Provornikova, E., Davila, J.M.: 2015, Evidence of thermal conduction suppression in a solar flaring loop by coronal seismology of slow-mode waves. *Astrophys. J. Lett.* **811**, L13. DOI.
- Wang, T., Ofman, O., Sun, X., Solanki, S.K., Davila, J.M.: 2018, Effect of transport coefficients on excitation of flare-induced standing slow-mode waves in coronal loops. *Astrophys. J.* **860**, 107. DOI.
- Wang, T., Ofman, O., Yuan, D., Reale, F., Kolotkov, D.Y., Srivastava, A.K.: 2021, Slow-mode magnetoacoustic waves in coronal loops. *Space Sci. Rev.* **217**, 2. DOI.
- Warren, H.P., Winebarger, A.R., Brooks, D.H.: 2010, Evidence for steady heating: observations of an active region core with Hinode and TRACE. *Astrophys. J.* **711**, 228. DOI.

- Weymann, R.: 1960, Heating of stellar chromospheres by shock waves. *Astrophys. J.* **132**, 452. [DOI](#).
- Zavershinskii, D.I., Kolotkov, D.Y., Nakariakov, V.N., Molevich, N.E., Ryashchikov, D.S.: 2019, Formation of quasi-periodic slow magnetoacoustic wave trains by the heating/cooling imbalance. *Phys. Plasmas* **26**, 082113. [DOI](#).
- Zavershinskii, D., Kolotkov, D., Riashchikov, D., Molevich, N.: 2021, Mixed properties of slow magnetoacoustic and entropy waves in a plasma with heating/cooling imbalance. *Solar Phys.* **296**, 96. [DOI](#).

**Publisher's Note** Springer Nature remains neutral with regard to jurisdictional claims in published maps and institutional affiliations.

Springer Nature or its licensor (e.g. a society or other partner) holds exclusive rights to this article under a publishing agreement with the author(s) or other rightsholder(s); author self-archiving of the accepted manuscript version of this article is solely governed by the terms of such publishing agreement and applicable law.